J. Cent. South Univ. (2021) 28: 2320−2332
DOI: https://doi.org/10.1007/s11771-021-4772-0

Springer

Effect of sintering temperature on microstructure and properties of glass-ceramics synthesized from waste cathode ray tubes funnel glass

LYU Jian-fang(吕建芳)[1, 3, 4], JIN Zhe-nan(金哲男)[2], MA Zhi-yuan(马致远)[1, 3, 4], YANG Hong-ying(杨洪英)[2]

1. Institute of Resources Comprehensive Utilization, Guangdong Academy of Sciences, Guangzhou 510650, China;
2. School of Metallurgy, Northeastern University, Shenyang 110819, China;
3. State Key Laboratory of Separation and Comprehensive Utilization of Rare Metals, Guangzhou 510650, China;
4. Guangdong Provincial Key Laboratory of Development and Comprehensive Utilization of Mineral Resources, Guangzhou 510650, China

Abstract: Waste cathode ray tube (CRT) funnel glass (FG) is an important part in the disposal of electrical and electronic waste (e-waste). A novel approach for efficient lead extraction and glass-ceramics synthesized from waste FG through collaboratively smelting FG with coal fly ash (CFA) is proposed. Glass-ceramics materials with 40 wt%−80 wt% FG additions were produced under sintering temperatures of 900−1000 °C. The microstructure and phase composition of the produced glass-ceramics were studied using X-ray diffraction (XRD) and scanning electron microscopy (SEM). The density, water absorption, Vicker hardness, chemical resistance and heavy metal leaching characteristics of the glass-ceramics were measured. The experimental results indicate that the samples can be crystallized at sintering temperatures of 900−1000 °C. An elevated sintering temperature is favorable for enhancing the degree of crystallization, while the crystallization process is inhibited at excessively high temperatures. Increasing FG addition can lead to the transformation of the main crystalline phase from diopside to gehlenite. Well-crystallized crystals were generated in the specimens with 50 wt%−70 wt% FG additions. The samples with 40 wt%, 50 wt%, 60 wt%, 70 wt%, 80 wt% FG addition exhibit the optimal chemical and physical properties at 975, 925, 950, 925 and 900 °C, respectively. Overall results demonstrate that this study provides a feasible strategy for reliably detoxifying and reusing waste FG and CFA.

Key words: coal fly ash; funnel glass; glass-ceramics; lead recovery; sintering temperature

Cite this article as: LYU Jian-fang, JIN Zhe-nan, MA Zhi-yuan, YANG Hong-ying. Effect of sintering temperature on microstructure and properties of glass-ceramics synthesized from waste cathode ray tubes funnel glass [J]. Journal of Central South University, 2021, 28(8): 2320−2332. DOI: https://doi.org/10.1007/s11771-021-4772-0.

1 Introduction

Lead-containing glasses, characterized by remarkable electrical performance and absorption of harmful rays, are widely used in the cathode ray tubes (CRT) for televisions and computer monitors. With the rapid development of display technology, traditional CRT displays have gradually been replaced by advanced displays [1], causing a large number of obsolete CRT displays to dispose. It was expected that CRT waste production could peak in

Foundation item: Project(2020GDASYL-20200103101) supported by the GDAS' Project of Science and Technology Development, China; Project(2020A1515010729) supported by the Natural Science Foundation of Guangdong Province, China; Project(2018YFC1902004) supported by the National Key R&D Program of China
Received date: 2020-08-07; **Accepted date:** 2021-04-23
Corresponding author: JIN Zhe-nan, PhD, Associate Professor; E-mail: jinzn@smm.neu.edu.cn; ORCID: https://orcid.org/0000-0002-3450-0594; MA Zhi-yuan, PhD, Senior Engineer; E-mail: mzy1988@163.com; ORCID: https://orcid.org/0000-0003-2216-2978

2015−2020 [2]. However, low-income consumers in Africa, Middle East, Eastern Europe, and Asia-Pacific still use CRT monitors because of the low cost of CRT sets [3]. The CRT funnel glass (FG) contains about 22%−25% PbO and accounts for 30% of a CRT's total weight [4]. The lead can be dissolved from the glass matrix of the FG when exposed to an acidic solution in landfills, posing a considerable threat to the environment and mankind [5].

Researches on the reutilization of waste FG have been intensively carried out in past decades, which generally can be classified into the reutilization as building materials, leaching techniques, and thermal treatments. Some researchers focus on using FG as secondary raw material to manufacture building materials, e.g., foam glass [6−8], glass-ceramics [9, 10], and cement mortar [11, 12], concrete [12−14], from the point of immobilizing Pb in the products. However, the toxic Pb that should be removed is also transformed into the products through the process, causing a potential threat to the environment and a waste of metal resources, which precludes the above-mentioned recycling methods. Thus, developments of techniques for lead extraction from FG have been widely performed for the safe disposal of waste CRTs, which can be classified into hydrometallurgical treatment (e.g., mechanical activation [15], hydrothermal sulfidisation [16], ultrasonically enhanced lead leaching [17], subcritical hydrothermal treatment [18], zeolite synthesis through hydrothermal treatment [19], alkaline leaching with mechanochemical reduction [20]) and pyrometallurgy treatment (e.g., carbon thermal reduction [21−24], thermal reduction with metallic iron [25], thermal reaction with SiC and TiN [26], combined thermal treatment and leaching processes [27, 28], and chloride volatilization [29]). By contrast, pyrometallurgy is more effective and promising in terms of extracting lead from the Pb-glass matrix since hydrometallurgical technology generally requires a high energy-consumption pretreatment and a long-process time but with a low lead recovery.

Glass-ceramic synthesis was confirmed as an efficient and applicable approach for the treatment of industrial residue (e.g., copper slag [30, 31], blast furnace slag [32, 33], nickel slag [34], stainless steel slag [35], coal fly ash (CFA) [36]) and tailings (e.g., gold-copper tailings [37], rare earth tailing [38], germanium tailings [39]) since the chemical compositions of the above-mentioned wastes are in accordance with the most common parent glass with ternary or quaternary systems. Besides, research on the glass-ceramic synthesis from waste CRT glass was also found in past decades [40−42]. However, these studies mainly focused on non-lead CRT panel glass, or directly using FG in producing glass-ceramics without lead extraction, which resulted in a waste of lead resources and a potential contaminant to the environment.

To produce glass-ceramics from FG, the introduction of other ingredient adjusters, e.g., CaO, Al_2O_3, and MgO, is required because the typical glass-ceramics systems used for construction materials are $CaO-Al_2O_3-SiO_2$, $MgO-Al_2O_3-SiO_2$, or $CaO-MgO-Al_2O_3-SiO_2$, while FG is mainly composed of SiO_2, PbO, K_2O, and Na_2O. CFA is an industrial by-product produced during the combustion of coal in thermal power plants, which contains a considerable amount of SiO_2, CaO, Al_2O_3, and Fe_2O_3. Thus, CFA can be used as a low-cost ingredient adjuster for the glass-ceramic synthesis from waste FG. Sintering method is commonly adopted for the production of glass-ceramics, which involves melt homogenization and sintering process. When using FG to produce glass-ceramics, the PbO in the FG can be recovered as metallic lead with the presence of reducing agents during the melt homogenization process. Therefore, it is reasonable to deduce that the glass-ceramic synthesis and lead extraction can be achieved simultaneously in the homogenization process. Based on the above considerations, we proposed a new approach for extracting lead and producing glass-ceramics from waste FG [10]. In brief, FG was collaboratively smelted with CFA, and the resultant homogeneous glass melt was quenched in water. Appropriate heat treatment was implemented to synthesize glass-ceramics from the quenched parent glass. The results provide a feasible strategy for detoxifying and reusing waste FG and CFA.

Based on the previous result, the influence of sintering temperature on crystallization behavior and physicochemical properties of glass-ceramics synthesized from waste FG and CFA was investigated. X-ray diffraction (XRD) and scanning electron microscopy (SEM) were employed to determine the changes in phase characteristics and

morphological properties of glass-ceramics samples obtained with 40 wt%−80 wt% FG additions. Moreover, the optimal sintering temperature was determined by the measurement of density, porosity, mechanical properties, chemical resistance, and leaching characteristics of the glass-ceramic samples.

2 Materials and methods

2.1 Materials

CRT FG was acquired from an appliance dismantling enterprise in Liaoning province, China. Anthracite was obtained from a metallurgic plant, and CFA was taken from a thermal power station in China. The chemical compositions of CFA and FG, determined by using X-ray fluorescence (XRF, PANalytical-Axios^{mAX}, Almelo, Netherlands), are given in Table 1. The main components of FG are SiO_2, PbO, K_2O, and Na_2O, and the main constitutes of CFA are SiO_2, CaO, and Al_2O_3, which are typical of the most common parent glass with ternary systems. XRD analysis of FG and CFA is shown in Figure 1. FG exhibits a total amorphous structure, and CFA shows a poorly crystallized state, where only peaks attributable to SiO_2 appear in the XRD pattern. The CaO used in the experiment is of analytical-grade. Anthracite with a fixed carbon content of 84.5% was employed as a reducing agent, and the carbon loading amount was determined by the molar ratio of C/PbO. Anthracite, FG, and CFA were crushed, milled, and dried for 24 h at 105°C.

Table 1 Chemical compositions of FG and CFA used for the experiment (wt%)

Sample	SiO_2	CaO	PbO	K_2O	Na_2O	Al_2O_3	MgO	Fe_2O_3	TiO_2
FG	53.39	4.53	20.25	9.90	4.44	3.69	1.75	0.3	—
CFA	56.92	10.00	—	2.23	1.23	21.51	1.42	3.78	1.20

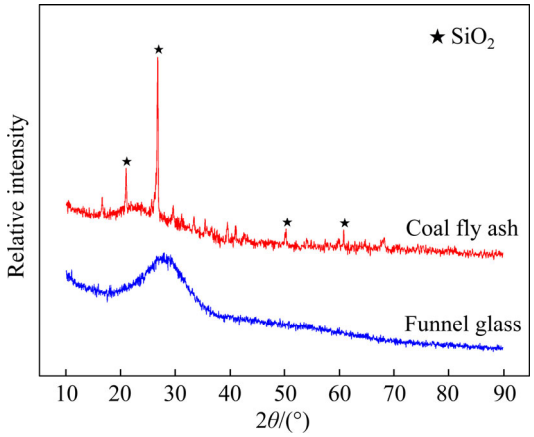

Figure 1 XRD patterns of FG and CFA

Samples with different FG additions, namely, 40 wt% FG-60 wt% CFA (FG40), 50 wt% FG-50 wt% CFA (FG50), 60 wt% FG-40 wt% CFA (FG60), 70 wt% FG-30 wt% CFA (FG70), and 80 wt% FG-20 wt% CFA (FG80), were prepared. Anthracite and CaO were introduced into the samples to gain a C/PbO ratio of 1.0 and a CaO/SiO_2 ratio of 0.4 determined in Ref. [10]. Afterwards, the prepared samples were homogenized by a blender mixer.

The fully mixed sample was loaded into an alumina crucible and then transferred to a $MoSi_2$ resistance furnace. The furnace was procedurally heated from room temperature to 1450 °C and kept for 2 h. Afterwards, the upper glass melt in the crucible was poured into cold water to ensure uniformity, and the metallic lead deposited at the bottom of the crucible and the residual glass were together quenched in water. After separating the metallic lead, the quenched glass particles were dried at 105 °C for 4 h and then ground into powder for producing glass-ceramic. The as-quenched glass was identified as parent glass. The flow chart of the whole process is shown in Figure 2.

Table 2 shows the chemical compositions of the parent glass. The content of PbO in the parent glass is below 0.6 wt% after reduction smelting. The contents of K_2O and Na_2O increase with FG addition, whereas the contents of Al_2O_3, Fe_2O_3, and TiO_2 show a continuous decrease. The concentrations of Na_2O in all glass samples are lower than the theoretical value due to the evaporation of Na_2O at high temperature [43].

2.2 Heat treatment

To prepare glass-ceramics, a cylindrical sample with a height of 5 mm and a diameter of 20 mm was obtained through cold-pressing of the parent glass powder at 30 MPa without using any adhesive. The cylindrical glass sample was dried for 6 h at 105 °C, placed in an alumina boat and heated to a given nucleation temperature at a rate of 10 °C/min in a SiC tube furnace. After treatment for 1 h, the sample was further heated to the desired sintering temperature at a rate of 3 °C/min, held for 2 h, and then cooled to room temperature along with the furnace. The nucleation temperature and sintering temperature were determined based on the DSC curve acquired in Ref. [10]. In brief, the nucleation temperature of samples FG40−FG80 was identified as 750 °C, and

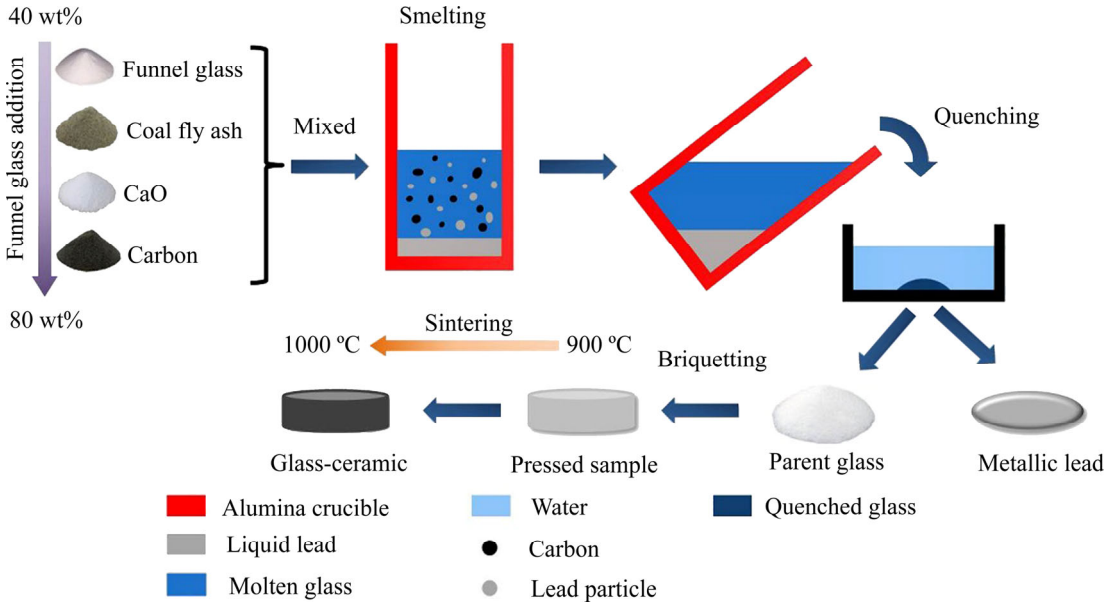

Figure 2 Flow chart of lead extraction and glass-ceramics synthesized from waste FG and CFA

Table 2 Chemical compositions of parent glass with various FG additions (wt%)

Sample	SiO_2	CaO	Al_2O_3	K_2O	Fe_2O_3	PbO	MgO	Na_2O	TiO_2
FG40	51.02	20.36	13.96	4.76	3.24	0.58	2.30	1.29	0.62
FG50	51.23	20.64	12.67	5.65	3.07	0.51	2.32	1.82	0.56
FG60	51.25	20.60	11.27	6.45	3.13	0.47	2.36	2.44	0.43
FG70	51.56	21.12	9.46	7.23	2.07	0.36	2.84	2.97	0.35
FG80	52.22	21.37	7.99	8.10	1.61	0.43	2.72	3.69	0.27

the sintering temperatures were selected to 900−1000 °C. The as-prepared glass-ceramic samples were partly crushed and ground into powder for chemical compositions analysis using XRF and atomic absorption spectroscopy (AAS, Z-2300, Hitachi, Japan).

2.3 X-ray diffraction and scanning electron microscopy analysis

XRD analysis (X'PERT PRO MPD/PW3040, PANalytical B.V. Corporation, Almelo, Netherlands) was carried out to explore the crystal phases of the nucleated glass-ceramic material. CuK radiation was used to collect the XRD patterns of the powder samples in the 2θ range of 10° to 80° for 10 min at 40 kV and 30 mA settings.

SEM (JSM-7800F JEOL, Tokyo, Japan) equipped with energy-dispersive X-ray spectroscope (EDS, INCA Energy 350, OXFORD) detector was employed to determine the microstructure characteristics of the sintered glass-ceramic samples at an acceleration voltage of 15 kV. Silicon carbide sandpaper was used to grind the samples, which were further polished with diamond paste to achieve a mirror-smooth surface. After being etched with HF solution (5 vol%) for 1.5 min, the polished samples were immediately rinsed with excess distilled water and then washed in ethanol for 2 min. The glass-ceramic samples were coated with carbon for microstructure analysis.

2.4 Properties tests

The conventional liquid displacement method based on the Archimedes principle was used to measure the water absorption (%) and density of the glass-ceramics samples, according to the procedure outlined in GB/T 9966.3-2001. In short, the sample was firstly weighed (m_0) and then immersed in distilled water at (20±2) °C for 48 h. The soaked sample was wiped with a wrung wet towel to remove the surface moisture and immediately weighed (m_1). Subsequently, the water-saturated sample was placed in a net basket, immersed in (20±2) °C distilled water, and then weighed in water (m_2). The apparent density

(ρ_a) and water absorption (W_a) are expressed in Eqs. (1) and (2):

$$\rho_a = \frac{m_0 \rho_w}{m_1 - m_2} \quad (1)$$

$$W_a = \frac{m_1 - m_0}{m_0} \times 100\% \quad (2)$$

where m_0 is the mass of the sample in air; m_1 is the mass of water-saturated sample in air; m_2 is the mass of water-saturated sample in water; and ρ_w is the density of distilled water at room temperature. After measuring the apparent density, the densities of the samples with a size of less than 45 mm were measured again. The porosity (P) was evaluated by the difference in density before and after grinding, according to Eq. (3):

$$P = \frac{\rho_b - \rho_a}{\rho_b} \times 100\% \quad (3)$$

where ρ_b is the density of the sintered sample after milling. The glass-ceramic samples were conducted with Vickers hardness measurements (KB3000BVRZ-SA, Shanghai Everone Precision Instruments Co., Ltd., China). Diamond paste was used to grind and polish the samples. The polished samples were measured with a load of 10 kg and an indentation time of 10 s. At least five points were tested in every test, and the results were averaged.

The chemical resistance was measured according to M. Erol's work [44]. To be specific, 2 g of granular samples were treated in 70 mL HNO_3 (10 wt%) and NaOH (10 wt%) solutions at 100 °C for 2 h, respectively. The specimens were soaked and then washed with distilled water, and were further dried at 105 °C for 6 h. Afterwards, the weight of the samples was measured, and the percentages of weight losses were calculated.

Toxic characteristic leaching procedure (TCLP) experiments were also performed on the synthesized glass-ceramic materials to characterize the leaching characteristics of heavy metals. First, 5.7 mL of glacial acetic acid was dissolved in 500 mL of deionized water to prepare the leaching solution (acetic acid buffer solution). Second, 64.3 mL of 1 mol/L NaOH solution was added, and the solution was diluted to 1 L. Third, the pH of the solution was adjusted to 4.93±0.05 using 1 mol/L HNO_3 or 1 mol/L NaOH. The ground glass-ceramic sample (<9.5 mm) was put in a leaching vial, and extraction fluid was added to obtain a liquid-solid ratio of 20 mL/g. The closed vial was stored at 25 °C for 18 h. A 0.45-μm filter was used to filter the resulting solutions and inductively coupled plasma-optical emission spectrometry (ICP-OES, Optima 8300DV, PerkinElmer, USA) was used to measure the concentrations of heavy metal ions in the leaching solution.

3 Results and discussion

3.1 Microstructural characterization of produced glass-ceramic samples

Figure 3 shows the XRD analysis results of glass-ceramic samples obtained at different sintering temperatures ranged from 900 to 1000 °C. For sample FG40, obvious diffraction peaks were observed at all tested temperature ranges, implying the occurrence of significant crystallization within the parent glass. The main crystal was identified as diopside ($Ca(Mg,Al)(Si,Al)_2O_6$, JCPDS card number: 00-025-0154), with anorthoclase ($Na_{0.71}K_{0.29}AlSi_3O_8$, JCPDS card number: 00-010-0361) as a secondary crystal phase. In addition, the higher background signals from 20° to 35° demonstrate the presence of amorphous glass phase in the produced glass-ceramics. When FG addition reaches 50 wt%, the crystalline phases of glass-ceramics transform into gehlenite ($Ca_2(Al(Al,Si)O_7$), JCPDS card number: 01-087-0968) and sanidine ($K_{0.47}Na_{0.43}Ca_{0.10}Al_{1.1}Si_{2.9}O_8$, JCPDS card number: 00-013-0456) (Figure 3(b)). With elevated sintering temperature, the diffraction peak of the sanidine phase gradually becomes weaker. Previous studies have identified crystalline phases such as gehlenite and diopside in the $CaO–Al_2O_3–SiO_2$ (CAS) type glass-ceramics [45]. The XRD pattern of the sample FG60 is similar to that of the sample FG50, where the crystal phases are sanidine and gehlenite (Figure 3(c)). The peaks of gehlenite are more pronounced at 950 and 1000 °C. Meanwhile, it is worth noting that the amorphous peak at 20°−35° decreases first and then increases with the increase of the sintering temperature, exhibiting its minimum at 950 °C, which suggests a favorable crystallinity. As FG addition increases to 70 wt% and 80 wt%, peaks attributable to $K_2MgSi_5O_{12}$ (JCPDS card number: 00-045-1499) become noticeable in the XRD patterns and dominate in FG80 sample, while the peaks for sanidine disappear. Gehlenite phase remains in the

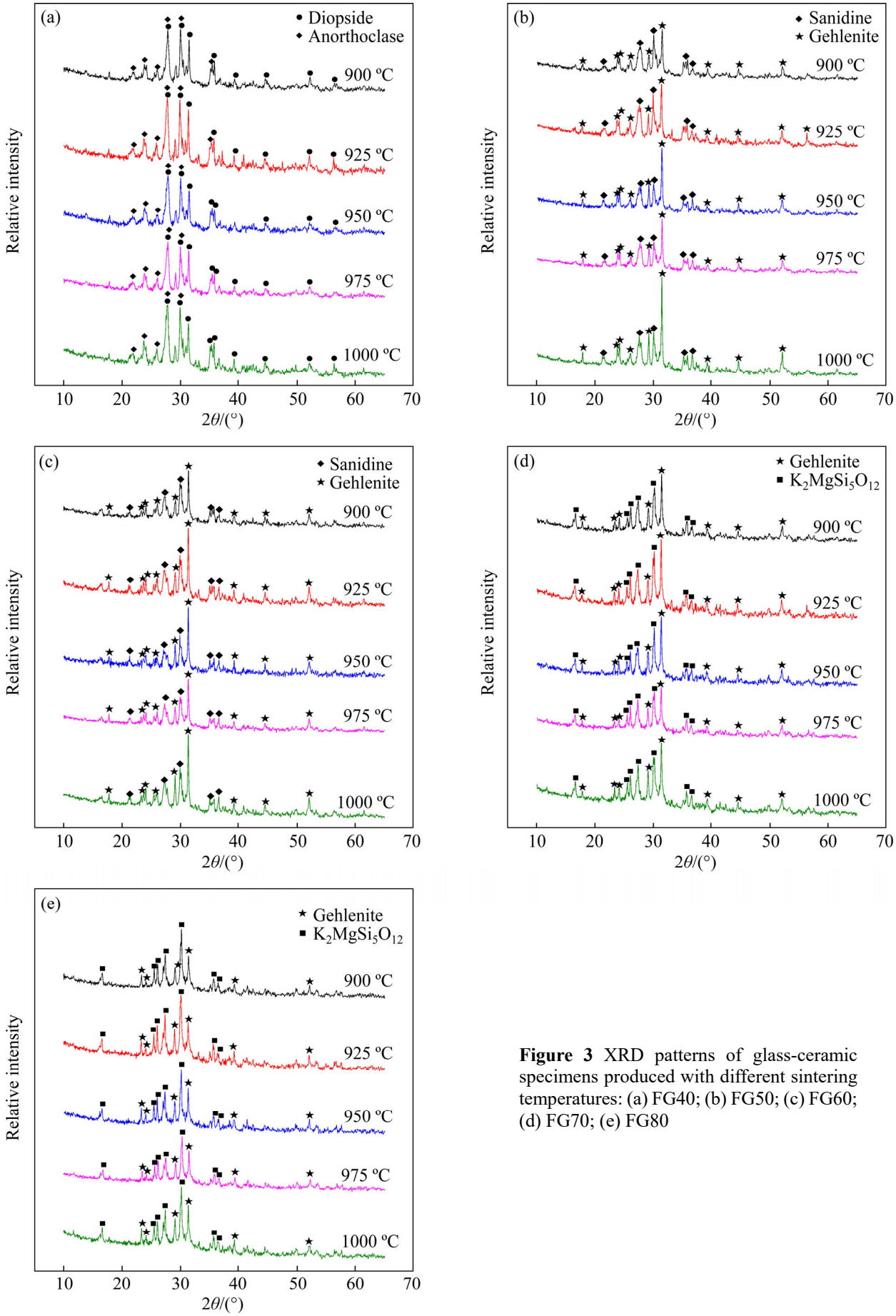

Figure 3 XRD patterns of glass-ceramic specimens produced with different sintering temperatures: (a) FG40; (b) FG50; (c) FG60; (d) FG70; (e) FG80

samples but with lower diffraction peak intensity. To sum up, at processing temperatures of 900−1000 °C, significant crystallization could occur within the samples FG40−FG80. Compared with samples FG40 and samples FG80, FG50, FG60 and FG70 exhibit a higher crystallinity. With FG addition, the diffraction peaks of gehlenite gradually weaken, while the Na- and K-containing heterogeneous crystal phases increase. This observation is consistent with the variation trend of the parent glass composition, that is, with the increase of FG addition, the content of Al_2O_3 gradually decreases, while Na_2O and K_2O increase.

Figure 4 shows the SEM images of surface morphologies of glass-ceramic samples FG40−FG80 produced with various sintering temperatures of 900−1000 °C. EDS analysis was performed in several regions on the surface of the specimens to check chemical homogeneity. The results show that the samples are generally homogenous, and segregation did not occur at higher temperatures. At lower sintering temperatures, the sample FG40 exhibits a low degree of crystallization, where the precipitated crystals with irregular shapes show an uneven distribution and varying grain sizes. Cracks appear between the grains, which may cause the mechanical strength of glass-ceramics to decrease. Besides, obvious voids were observed on the surface of glass-ceramic samples after being treated with HF due to the presence of amorphous glass, which is prone to be corroded by HF compared with the crystals. The quantity of crystal in glass-ceramics increases with sintering temperature. The grains are spherical, with the largest size at 975 °C.

Analogous to the sample FG40, the degree of crystallization of the sample FG50 increases with the increasing sintering temperature. Spherical shape crystals with a size of 100−300 nm were observed in the SEM image. When the temperature reaches 1000 °C, the number of crystal grains decreases, and a mass of glass phases exist in the sample with crystals embedded in the glass matrix. Generally, the crystallization process of glass-ceramics includes two stages, namely, crystal nucleation and crystal growth. The rate of nucleation and crystal growth are functions of undercooling and viscosity. The hindrance of viscosity to particle diffusion limits the crystallization rate, especially the crystal nuclei grow rate. Previous studies have shown that temperature has two effects on sintering. On the one hand, the

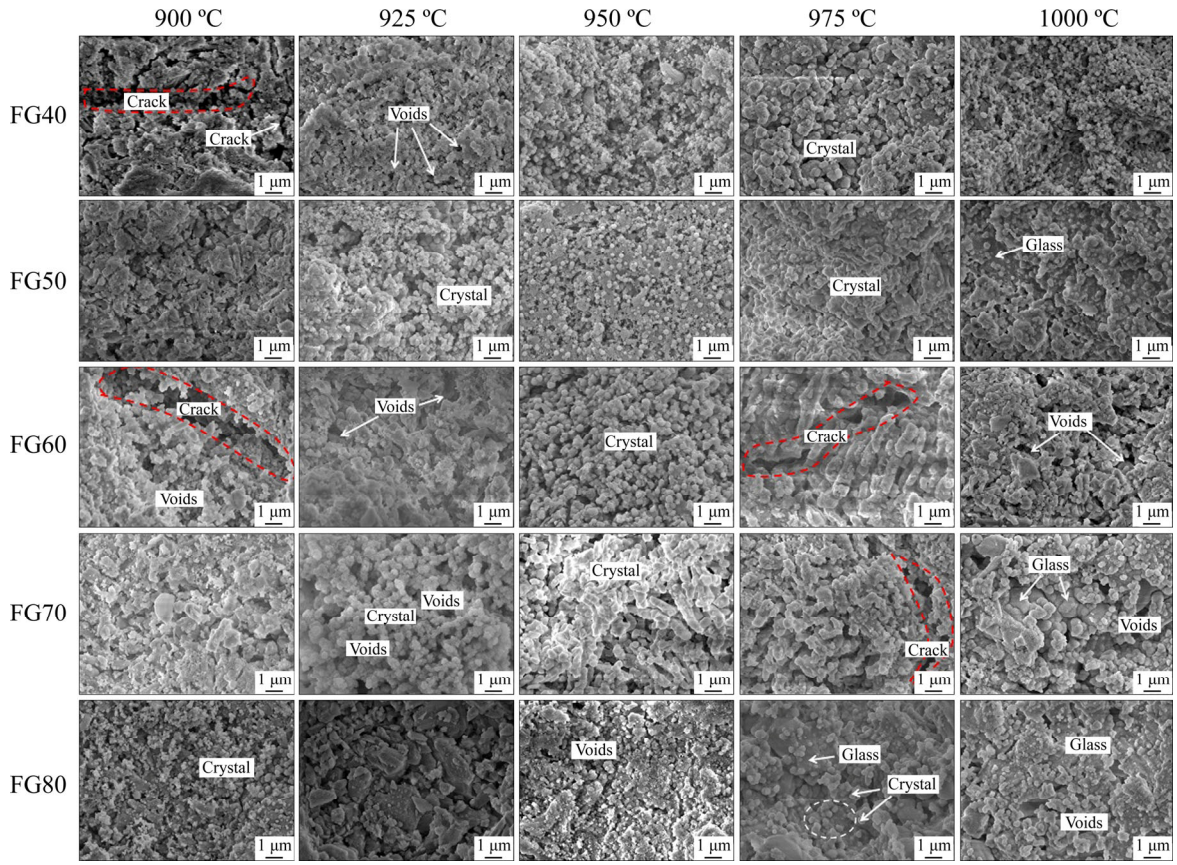

Figure 4 SEM images of glass-ceramic specimens produced with various sintering temperatures

glass viscosity decreases with the increase of sintering temperature, which promotes the viscous flow mass transfer of the glass liquid phase, thereby resulting in a dense sintering of glass-ceramics. On the other hand, as the temperature rises, the crystallization degree of the glass-ceramic increases rapidly. The elevated viscosity of the liquid glass resulted from the precipitation of the crystal phase causes high resistance to crystallization, which inhibits the further sintering process. Therefore, the FG50 sample exhibits an inferior crystallinity at 1000 °C, because this temperature significantly exceeds the crystallization temperature of 953.17 °C.

Sample FG60 shows a low degree of crystallization at 900 and 925 °C. Crystal grains with uneven size and distribution are observed in the sample. As the sintering temperature increases, the crystals in the sample grow, and the number of crystal increases. The crystallites of the glass-ceramics are densely distributed, and their sizes tend to be uniform. At 975 °C, club-shaped crystals with a size in the range of 1−2 μm in length are homogeneously dispersed within the glass matrix. However, a further increase of sintering temperature causes a reduced degree of crystallization of the glass-ceramic. The crystals exhibit an uneven size and seem to combine with a glass phase. The variation trend of FG70 is consistent with FG60, where the sample shows a poor crystallinity at a lower sintering temperature, and then the crystallization degree increases by the elevated temperature, reaching the optimum at 950°C, followed by a decrease with a further increase of sintering temperature.

For sample FG80, it is noted that agglomerated tiny crystals 80−250 nm long were sparsely embedded in the glass matrix, and most parent glasses remained un-nucleated at the tested temperature range. Some cracks were observed in the glass matrix, which may lead to high porosity and poor mechanical properties.

To summarize, the SEM observations are consistent with the XRD results, confirming a relatively high crystallization degree in samples FG50−FG70 and a worse crystallization state in samples FG40 and FG80. Increasing sintering temperature can enhance the crystallization degrees of samples FG40−FG70, but excessive temperature exerts an adverse effect on the crystallization.

3.2 Physical and mechanical properties of produced glass-ceramics samples

Figures 5(a)−(d) describe the influence of sintering temperature on apparent density, relative density, water absorption, and hardness of glass-ceramics specimens, respectively. The apparent densities of glass-ceramic samples FG40−FG70 increase as the sintering temperature increases and begin to decrease after reaching a certain value. The densities of samples FG40−FG70 reach their maximum values at 975, 925, 950 and 925 °C, which were 2.42, 2.51, 2.59 and 2.69 g/cm^3, respectively. In comparison, the density of sample FG80 decreases continuously with the increasing temperature, exhibiting its maximum of 2.66 g/cm^3 at 900 °C. According to previous studies, the density of glass-ceramics correlates well with the crystallization degree. The occurrence of crystallization can promote the formation of more dense crystal structures in the sample and decrease the pores between the crystals, resulting in an increased density and a reduced water absorption of the sample [44]. It is observed that both samples FG40 an FG80 show their best densities at the sintering temperature below crystallization temperature, with differentials ranging from 12.5−28.2 °C. This is because the crystallization degree was not only influenced by the sintering temperature. Other factors, such as sintering time, glass viscosity, and glass particle size, can also exert an effect on the crystallization of the sample. Thus, the optimal crystallization degree may not be accurately obtained at crystallization temperature. The varying differentials among different samples may be attributed to deviation resulted from the glass quenching process, which is manually operated by pouring the melt into water using a hawkbill. To determine the variation trend of density among different samples, the relative densities (ρ_r) were calculated by considering the deviation caused by composition change. The relative density is expressed as follows:

$$\rho_r = \frac{\rho_a}{\sum_x \varpi_x M_x} \tag{4}$$

where ρ_a is the apparent density of the glass-ceramic sample; ω_x donates the mass fraction of metallic oxide in the glass sample; M_x donates the relative molecular mass of metallic oxide in the glass sample.

The results shown in Figure 5(b) indicate that

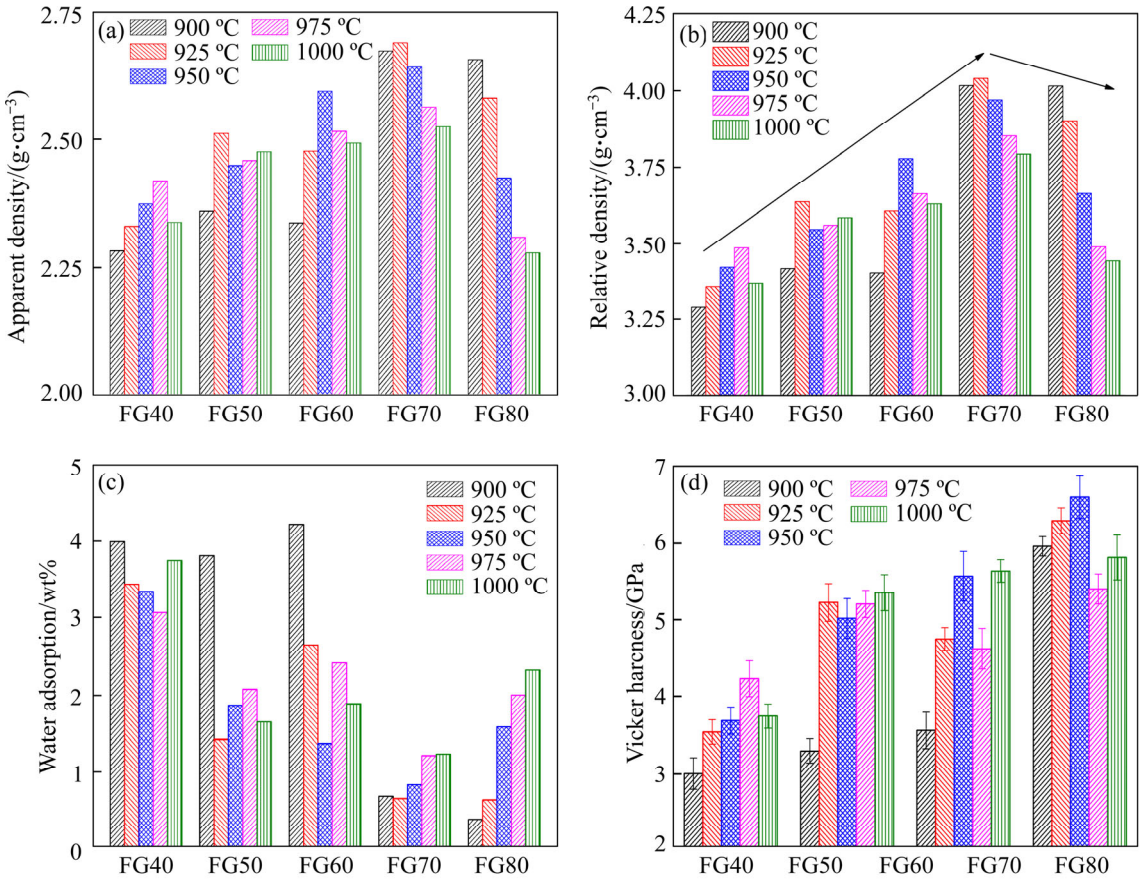

Figure 5 Effect of sintering temperature on: (a) Apparent density; (b) Relative density; (c) Water absorption; (d) Vicker hardness of produced glass-ceramic specimens

the relative density of glass-ceramics increases by the addition of FG. This can be attributed to the low softening point of the glass, which provides a large amount of liquid phase during the sintering process and therefore reduces the viscosity of the parent glass. As a consequence, the diffusion of ions in glass-ceramics is accelerated, thereby promoting the crystal nucleation and growth. The precipitation of the crystalline phase leads to the shrinkage of pores in the sample to form a dense structure. However, excessive FG addition can inhibit the sintering process due to the presence of a high level of brittle glass. The variation trend of water absorption is opposite to that of density (Figure 5(c)), that is, the water absorption initially decreases and then increases with the temperature for samples FG40−FG70, while it shows a continuous decrease for the FG80 sample.

Figure 5(d) presents the Vickers hardness of samples FG40−FG80 as a function of sintering temperature. The Vickers hardness of the sample FG40 increases first and then decreases with increasing temperature, reaching a maximum of 4.23 GPa at 975 °C. The hardness of FG50 sample shows a significant increase as the temperature varies from 900 to 925°C and then keeps at a steady level. The sample FG60 exhibits a favorable compressive property at sintering temperatures of 950 and 1000 °C, where the hardness is 568 and 5.64 GPa, respectively. As FG addition reaches 70 wt%, a remarkable compressive property up to 6.60 GPa was obtained at 950 °C. Hardness value for FG80 sample is unavailable because fragmentation occurred around the indentation during the measurement, and the indentation area could not be read. As indicated by the chemical compositions of FG and CFA, the content of R_2O in the parent glass gradually increases by the addition of FG, while the contents of Fe_2O_3 and TiO_2 decrease. R_2O acts as a network breaker to provide free oxygen to the glass matrix, thereby promoting the depolymerization of the silicate network structure and reducing the viscosity of the glass. Moreover, the sintering activation energy of the glass-ceramic sample and the initial sintering temperature can be decreased by R_2O, thereby facilitating the sintering process [46].

Therefore, the increase of FG addition can promote the sintering to some extent, leading to the enhancement of the physicochemical properties. Further introduction of FG, however, can inhibit the sintering process because of the high level of R_2O. When FG addition increases to 80 wt%, the sintering and crystallization occurred almost simultaneously within the sample. Consequently, the viscosity of the liquid phase increases rapidly due to the precipitation of crystals, thereby reducing the sintering rate. Most of the brittle glass phase remains in the sample, causing a decreased compressive property.

3.3 Chemical resistance and leaching characteristics of produced glass-ceramic samples

The acid resistance is an important indicator to determine the feasibility of using glass-ceramics as a building exterior wall material. Thus, the chemical durabilities of the glass-ceramic materials were measured, and the results are listed in Table 3. Glass-ceramic is mainly composed of a crystal phase and a glass phase. The acid resistance of the crystal phase is superior to that of the glass phase, so the acid resistance is mainly determined by the degree of crystallization. The elevated crystallization degree results in the generation of more crystals in the sample. Besides, the enhancement of the crystallization degree could lead to a more dense structure in order that the pore space between crystals gradually decreased. As a result, the reaction specific surface area decreased, and resultant good stability in acid solution was obtained. The variation trend of acid resistance of glass-ceramics is generally in accordance with the density. That is, as the sintering temperature increases, the corrosion resistance of glass-ceramics increases first and then decreases. The optimal acid resistances of samples FG40−FG80 were obtained at 975, 925, 950, 925 and 925 °C, respectively. Additionally, it is obvious that the produced glass-ceramic samples possess higher resistance to alkali solutions than acidic solutions because the glassy matrix is more easily leached in the acidic solutions.

Table 3 Chemical resistances of sintered glass-ceramic samples

Solvent (10%)	*T*/°C	Mass loss/wt%				
		FG40	FG50	FG60	FG70	FG80
HNO_3	900	7.83	4.53	5.45	2.43	3.83
	925	5.31	2.61	3.82	2.37	3.48
	950	4.73	3.29	3.28	3.16	4.49
	975	3.42	3.77	3.71	3.46	4.86
	1000	5.12	3.96	3.57	3.52	5.59
NaOH	900	0.31	0.18	0.47	0.02	0.18
	925	0.20	0.01	0.23	0.01	0.15
	950	0.15	0.03	0.04	0.05	0.12
	975	0.06	0.05	0.11	0.04	0.33
	1000	0.18	0.05	0.21	0.03	0.62

TCLP measurement was performed on the glass-ceramic samples synthesized at the optimal sintering temperatures. The results shown in Table 4 indicate that the contents of Cu and Cr in the leaching solution were lower than the detection limit. A small amount of Pb and Zn was detected in the filtrate, which was well below the regulatory limits of the US Environmental Protection Agency (US-EPA). This result proves that the residual heavy metals were successfully immobilized in the sintered glass-ceramic materials, and the prepared glass-ceramic samples are non-toxic materials.

Table 4 TCLP results of sintered glass-ceramic samples (mg/L)

Sample	Pb	Zn	Cu	Cr
FG40	0.11	0.07	N.D	N.D
FG50	0.03	0.02	N.D	N.D
FG60	N.D*	0.09	N.D	N.D
FG70	N.D	0.04	N.D	N.D
FG80	0.06	0.04	N.D	N.D
US-EPA limit	5	100	15	5

N.D: Values are below detection limit.

4 Conclusions

This study proposes an innovative method for extracting lead and synthesizing glass-ceramics from waste FG and CFA. The effects of sintering temperatures on phase, structure, and properties of glass-ceramics were studied by XRD, SEM, and physicochemical property measurements. The following conclusions can be drawn:

1) Significant crystallization could occur within samples FG40−FG80 after being sintered at 900−1000 °C. Compared with samples FG40 and samples FG80, FG50, FG60 and FG70 showed a higher degree of crystallization. By the addition of

FG, the main crystal phase of glass-ceramic transformed from diopside to gehlenite. The crystal phase of glass-ceramics is mainly spherical. The degree of crystallization gradually increased with elevated sintering temperature, and then decreased when the temperature reached a certain value.

2) The densities of glass-ceramic samples FG40−FG70 increased with the sintering temperature, followed by a decrease after a certain temperature, while the sample FG80 showed a continuous decrease. The highest densities of the prepared glass-ceramic samples were generally obtained at the sintering temperature closed to the crystallization temperature. The increase of FG addition can enhance the density of glass-ceramics due to the presence of low melting point constituent in FG. The variation trend of water absorption is opposite to that of density.

3) The chemical resistance of produced glass-ceramics was relevant to the density, that is, specimens FG40−FG80 showed desirable chemical resistance at the optimal density. The resistance of the produced glass-ceramic samples to alkali solutions is stronger than to the acidic solutions. TCLP test confirmed that the synthesized materials were non-hazardous. Engineering and construction applications of the superior glass-ceramic products were proved to be possible by the physical and mechanical properties measurements, chemical resistance tests, and leaching characteristics of heavy metals.

Contributors

LYU Jian-fang and YANG Hong-ying provided the concept. LYU Jian-fang conducted the literature review and wrote the first draft of the manuscript. JIN Zhe-nan offered the materials. LYU Jian-fang, JIN Zhe-nan and MA Zhi-yuan carried out experiments, performed data analysis, and contributed to the paper editing. All authors replied to reviewers' comments and revised the final version.

Conflict of interest

LYU Jian-fang, JIN Zhe-nan, MA Zhi-yuan, and YANG Hong-ying declare that they have no conflict of interest.

References

[1] GONG Yu, TIAN Xiang-miao, WU Yu-feng, TAN Zhe, LÜ Lei. Recent development of recycling lead from scrap CRTs: A technological review [J]. Waste Management, 2016, 57: 176−186. DOI: 10.1016/j.wasman.2015.09.004.

[2] YOSHIDA A, TERAZONO A, BALLESTEROS F C Jr, NGUYEN D Q Jr, SUKANDAR S Jr, KOJIMA M Jr, SAKATA S Jr. E-waste recycling processes in Indonesia, the Philippines, and Vietnam: A case study of cathode ray tube TVs and monitors [J]. Resources, Conservation and Recycling, 2016, 106: 48−58. DOI: 10.1016/j.resconrec.2015.10.020.

[3] SINGH N, WANG Jie-cong, LI Jin-hui. Waste cathode rays tube: An assessment of global demand for processing [J]. Procedia Environmental Sciences, 2016, 31: 465−474. DOI: 10.1016/j.proenv.2016.02.050.

[4] GREGORY J R, NADEAU M C, KIRCHAIN R E. Evaluating the economic viability of a material recovery system: The case of cathode ray tube glass [J]. Environmental Science & Technology, 2009, 43(24): 9245−9251. DOI: 10.1021/es901341n.

[5] YOT P G, MÉAR F O. Characterization of lead, Barium and strontium leachability from foam glasses elaborated using waste cathode ray-tube glasses [J]. Journal of Hazardous Materials, 2011, 185(1): 236−241. DOI: 10.1016/j.jhazmat.2010.09.023.

[6] ØSTERGAARD M B, PETERSEN R R, KÖNIG J, BOCKOWSKI M, YUE Yuan-zheng. Foam glass obtained through high-pressure sintering [J]. Journal of the American Ceramic Society, 2018, 101(9): 3917−3923. DOI: 10.1111/jace.15574.

[7] PETERSEN R R, KÖNIG J, IVERSEN N, ØSTERGAARD M B, YUE Yuan-zheng. The foaming mechanism of glass foams prepared from the mixture of Mn_3O_4, carbon and CRT panel glass [J]. Ceramics International, 2021, 47(2): 2839−2847. DOI: 10.1016/j.ceramint.2020.09.138.

[8] ZHANG Qiu-ping, HE Feng, SHU Hao, QIAO Ye-chu, MEI Shu-xia, JIN Ming-fang, XIE Jun-lin. Preparation of high strength glass ceramic foams from waste cathode ray tube and germanium tailings [J]. Construction and Building Materials, 2016, 111(15): 105−110. DOI: 10.1016/j.conbuildmat.2016.01.036.

[9] XU Bao-qiang, WANG Feng-kang, YANG Jia, YANG Bin, ZHAO Jin-yang. Enhancing Pb removal and synthesizing glass-ceramics from waste CRTs funnel glass by red mud [J]. Journal of Sustainable Metallurgy, 2020, 6(3): 367−374. DOI: 10.1007/s40831-020-00282-7.

[10] LYU Jian-fang, YANG Hong-ying, JIN Zhe-nan, ZHAO Ming-lei. Lead extraction and glass-ceramics synthesis from waste cathode ray tube funnel glass through cooperative smelting process with coal fly ash [J]. Waste Management, 2018, 76: 687−696. DOI: 10.1016/j.wasman.2018.03.019.

[11] LI Jiang-shan, GUO Ming-zhi, XUE Qiang, POON C S. Recycling of incinerated sewage sludge ash and cathode ray tube funnel glass in cement mortars [J]. Journal of Cleaner Production, 2017, 152: 142−149. DOI: 10.1016/j.jclepro.2017.03.116.

[12] LIU Tie-jun, SONG Wen, ZOU Du-jian, LI Lei. Dynamic mechanical analysis of cement mortar prepared with recycled cathode ray tube (CRT) glass as fine aggregate [J]. Journal of Cleaner Production, 2018, 174: 1436−1443. DOI: 10.1016/j.jclepro.2017.11.057.

[13] LIU Tie-jun, WEI Hui-nan, ZOU Du-jian, ZHOU Ao, JIAN Hong-shu. Utilization of waste cathode ray tube funnel glass for ultra-high performance concrete [J]. Journal of Cleaner Production, 2020, 249: 119333. DOI: 10.1016/j.jclepro.2019.119333.

[14] WEI Hui-nan, ZHOU Ao, LIU Tie-jun, ZOU Du-jian, JIAN Hong-shu. Dynamic and environmental performance of eco-friendly ultra-high performance concrete containing waste cathode ray tube glass as a substitution of river sand [J]. Resources, Conservation and Recycling, 2020, 162: 105021. DOI: 10.1016/j.resconrec.2020.105021.

[15] SINGH N, LI Jin-hui, ZENG Xian-lai. An innovative method for the extraction of metal from waste cathode ray tubes through a mechanochemical process using 2-[bis(carboxymethyl)amino]acetic acid chelating reagent [J]. ACS Sustainable Chemistry & Engineering, 2016, 4(9): 4704−4709. DOI: 10.1021/acssuschemeng.6b00875.

[16] YUAN Wen-yi, MENG Wen, LI Jin-hui, ZHANG Cheng-long, SONG Qing-bin, BAI Jian-feng, WANG Jing-wei, LI Ying-shun. Lead recovery from scrap cathode ray tube funnel glass by hydrothermal sulphidisation [J]. Waste Management & Research, 2015, 33(10): 930−936. DOI: 10.1177/0734242x15597777.

[17] SATERLAY A J, WILKINS S J, COMPTON R G. Towards greener disposal of waste cathode ray tubes via ultrasonically enhanced lead leaching [J]. Green Chemistry, 2001, 3(4): 149−155. DOI: 10.1039/b102671m.

[18] MIYOSHI H, CHEN Dan-ping, AKAI T. A novel process utilizing subcritical water to remove lead from wasted lead silicate glass [J]. Chemistry Letters, 2004, 33(8): 956−957. DOI: 10.1246/cl.2004.956.

[19] YAO Zhi-tong, WU Dai-dai, LIU Jie, WU Wei-hong, ZHAO Hong-ting, TANG Jun-hong. Recycling of typical difficult-to-treat e-waste: Synthesize zeolites from waste cathode-ray-tube funnel glass [J]. Journal of Hazardous Materials, 2017, 324: 673−680. DOI: 10.1016/j.jhazmat.2016.11.041.

[20] ZHANG Cheng-long, ZHUANG Li-li, YUAN Wen-yi, WANG Jing-wei, BAI Jian-feng. Extraction of lead from spent leaded glass in alkaline solution by mechanochemical reduction [J]. Hydrometallurgy, 2016, 165: 312−317. DOI: 10.1016/j.hydromet.2016.01.017.

[21] XING Ming-fei, FU Ze-gang, WANG Ya-ping, WANG Jing-yu, ZHANG Zhi-yuan. Lead recovery and high silica glass powder synthesis from waste CRT funnel glasses through carbon thermal reduction enhanced glass phase separation process [J]. Journal of Hazardous Materials, 2017, 322: 479−487. DOI: 10.1016/j.jhazmat.2016.10.012.

[22] SINGH N, LI Jin-hui. An efficient extraction of lead metal from waste cathode ray tubes (CRTs) through mechano-thermal process by using carbon as a reducing agent [J]. Journal of Cleaner Production, 2017, 148: 103−110. DOI: 10.1016/j.jclepro.2017.01.122.

[23] HU Biao, HUI Wen-long. Lead recovery from waste CRT funnel glass by high-temperature melting process [J]. Journal of Hazardous Materials, 2018, 343: 220−226. DOI: 10.1016/j.jhazmat.2017.09.034.

[24] LV Jian-fang, YANG Hong-ying, JIN Zhe-nan, MA Zhi-yuan, SONG Yan. Feasibility of lead extraction from waste Cathode-Ray-Tubes (CRT) funnel glass through a lead smelting process [J]. Waste Management, 2016, 57: 198−206. DOI: 10.1016/j.wasman.2016.05.010.

[25] LU Xing-wen, SHIH Kai-min, LIU Cheng-shuai, WANG Fei. Extraction of metallic lead from cathode ray tube (CRT) funnel glass by thermal reduction with metallic iron [J]. Environmental Science & Technology, 2013, 47(17): 9972−9978. DOI: 10.1021/es401674d.

[26] YOT P G, MÉAR F O. Lead extraction from waste funnel cathode-ray tubes glasses by reaction with silicon carbide and titanium nitride [J]. Journal of Hazardous Materials, 2009, 172(1): 117−123. DOI: 10.1016/j.jhazmat.2009.06.137.

[27] OKADA T. Water-soluble lead in cathode ray tube funnel glass melted in a reductive atmosphere [J]. Journal of Hazardous Materials, 2016, 316: 43−51. DOI: 10.1016/j.jhazmat.2016.05.013.

[28] OKADA T. Lead extraction from cathode ray tube funnel glass melted under different oxidizing conditions [J]. Journal of Hazardous Materials, 2015, 292: 188−196. DOI: 10.1016/j.jhazmat.2015.03.009.

[29] GRAUSE G, TAKAHASHI K, YOSHIOKA T. Thermogravimetric investigation of the lead volatilization from waste cathode-ray tube glass [J]. Recycling, 2016, 1(1): 111−121. DOI: 10.3390/recycling1010111.

[30] YANG Zhi-hong, LIN Qiao, XIA Ji-xiang, HE Yong, LIAO Guang-dong, KE Yi. Preparation and crystallization of glass-ceramics derived from iron-rich copper slag [J]. Journal of Alloys and Compounds, 2013, 574: 354−360. DOI: 10.1016/j.jallcom.2013.05.091.

[31] YANG Zhi-hong, LIN Qiao, LU Sheng-chun, HE Yong, LIAO Guang-dong, KE Yi. Effect of CaO/SiO_2 ratio on the preparation and crystallization of glass-ceramics from copper slag [J]. Ceramics International, 2014, 40(5): 7297−7305. DOI: 10.1016/j.ceramint.2013.12.071.

[32] HE Dong-feng, GAO Chong, PAN Jiang-tao, XU An-jun. Preparation of glass-ceramics with diopside as the main crystalline phase from low and medium titanium-bearing blast furnace slag [J]. Ceramics International, 2018, 44(2): 1384−1393. DOI: 10.1016/j.ceramint.2017.09.019.

[33] ZHAO Yan, CHEN Deng-fu, BI Yan-yan, LONG Mu-jun. Preparation of low cost glass-ceramics from molten blast furnace slag [J]. Ceramics International, 2012, 38(3): 2495−2500. DOI: 10.1016/j.ceramint.2011.11.018.

[34] WANG Zhong-jie, NI Wen, JIA Yan, ZHU Li-ping, HUANG Xiao-yan. Crystallization behavior of glass ceramics prepared from the mixture of nickel slag, blast furnace slag and quartz sand [J]. Journal of Non-Crystalline Solids, 2010, 356(31, 32): 1554−1558. DOI: 10.1016/j.jnoncrysol.2010.05.063.

[35] FAN Wen-di, YANG Qiang-wei, GUO Bin, LIU Bo, ZHANG Shen-gen. Crystallization mechanism of glass-ceramics prepared from stainless steel slag [J]. Rare Metals, 2018, 37(5): 413−420. DOI: 10.1007/s12598-018-1030-1.

[36] ZHU Meng-guang, JI Ru, LI Zhong-min, WANG Hao, LIU Li-li, ZHANG Zuo-tai. Preparation of glass ceramic foams for thermal insulation applications from coal fly ash and waste glass [J]. Construction and Building Materials, 2016, 112: 398−405. DOI: 10.1016/j.conbuildmat.2016.02.183.

[37] YE Chu-qiao, HE Feng, SHU Hao, QI Hao, ZHANG Qiu-pin, SONG Pei-yu, XIE Jun-lin. Preparation and properties of sintered glass-ceramics containing Au-Cu tailing waste [J].

Materials & Design, 2015, 86: 782−787. DOI: 10.1016/j.matdes.2015.07.173.

[38] ZHAO Tuan, LI Bao-wei, GAO Zhan-yong, CHANG Da-qiang. The utilization of rare earth tailing for the production of glass-ceramics [J]. Materials Science and Engineering: B, 2010, 170(1−3): 22−25. DOI: 10.1016/j.mseb.2010.02.019.

[39] ZHANG Qiu-ping, HE Feng, SHU Hao, QIAO Ye-chu, MEI Shu-xia, JIN Ming-fang, XIE Jun-lin. Preparation of high strength glass ceramic foams from waste cathode ray tube and germanium tailings [J]. Construction and Building Materials, 2016, 111: 105−110. DOI: 10.1016/j.conbuildmat.2016.01.036.

[40] GUO H W, GONG Y X, GAO S Y. Preparation of high strength foam glass-ceramics from waste cathode ray tube [J]. Materials Letters, 2010, 64(8): 997−999. DOI: 10.1016/j.matlet.2010.02.006.

[41] ANDREOLA F, BARBIERI L, CORRADI A, LANCELLOTTI I, FALCONE R, HREGLICH S. Glass-ceramics obtained by the recycling of end of life cathode ray tubes glasses [J]. Waste Management, 2005, 25(2): 183−189. DOI: 10.1016/j.wasman.2004.12.007.

[42] BERNARDO E, ANDREOLA F, BARBIERI L, LANCELLOTTI I. Sintered glass-ceramics and glass-ceramic matrix composites from CRT panel glass [J]. Journal of the American Ceramic Society, 2005, 88(7): 1886−1891. DOI: 10.1111/j.1551-2916.2005.00380.x.

[43] TONG Z F, QIAO J L, JIANG X Y. Kinetics of Na_2O evaporation from CaO-Al_2O_3-SiO_2-MgO-TiO_2-Na_2O slags [J]. Ironmaking & Steelmaking, 2017, 44(4): 237−245. DOI: 10.1080/03019233.2016.1210354.

[44] EROL M, KÜÇÜKBAYRAK S, ERSOY-MERIÇBOYU A. Production of glass-ceramics obtained from industrial wastes by means of controlled nucleation and crystallization [J]. Chemical Engineering Journal, 2007, 132(1−3): 335−343. DOI: 10.1016/j.cej.2007.01.029.

[45] JIN De -luan, LI Ai-min, SU Tong, CUI Xiao-bo. Synthesis of nucleated glass-ceramics using oil shale fly ash [J]. Journal of Hazardous Materials, 2010, 173(1−3): 427−432. DOI: 10.1016/j.jhazmat.2009.08.099.

[46] CHENG Jin-shu, WANG Huai-de, ZHAO Qian, YUAN Jian. Influence of Na_2O content on sintering and devitrification of glass-ceramic decorated material [J]. Journal of Wuhan University of Technology, 1996, 18(1): 30−32. (in Chinese)

(Edited by ZHENG Yu-tong)

中文导读

烧结温度对废弃阴极射线管锥玻璃制备微晶玻璃的结构及性能的影响

摘要：废弃阴极射线管(CRT)锥玻璃(FG)是电子电气废物（电子废物）处置中的重要组成部分。本文提出了一种通过锥玻璃与粉煤灰(CFA)协同冶炼从锥玻璃中高效提取铅并制备微晶玻璃的新方法。在 FG 加入量 40 wt%~80 wt%、烧结温度 900~1000 °C 的条件下制备了微晶玻璃材料。通过 X 射线衍射(XRD)和扫描电子显微镜(SEM)研究了微晶玻璃的微观结构和相组成。测量了微晶玻璃的密度、吸水率、维氏硬度、化学抗性和重金属浸出特性。实验结果表明，样品可以在 900~1000 °C 的烧结温度下产生晶化。较高的烧结温度有利于提高结晶度，但温度过高会抑制析晶。随着 FG 添加量的增加，主晶相从透辉石转变为钠钙石。FG 加入量为 50 wt%~70 wt%的样品结晶度较高。FG 加入量为 40 wt%、50 wt%、60 wt%、70 wt%、80 wt%的样品分别在 975、925、950、925 和 900 °C 下达到最佳的化学和物理性能。结果表明，本文提出的方法可实现废弃锥玻璃和粉煤灰的无害化及再生利用。

关键词：粉煤灰；锥玻璃；微晶玻璃；铅回收；烧结温度